

# MODELING OF A CO<sub>2</sub> THERMOSYPHON FOR A GROUND SOURCE HEAT PUMP APPLICATION

*Stefan Bertsch, Graduate Student, Ray W. Herrick Laboratories,  
Eckhard A. Groll, Associate Professor, Ray W. Herrick Laboratories  
Kevin Whitacre, Graduate Student, School of Mechanical Engineering  
Purdue University, West Lafayette, IN 47907, USA*

## ABSTRACT

Ground source heat pumps provide high efficiency operation during the space heating season, even during time periods of very low or rapidly varying outdoor temperatures, due to the use of the ground as a stable-temperature heat source. Up to now most ground source heat pump systems rely on a brine solution in a secondary fluid loop to extract heat from the soil. Recently, a new concept has gained interest which uses a closed, self-circulating CO<sub>2</sub> thermosyphon to extract heat from the soil. Advantages of this system are the higher efficiency compared to secondary fluid loops and environmentally friendliness. The disadvantage of this system is that it only works in heating and not in cooling mode. The scope of the analysis presented in this paper is to model the two-phase counter-current annular flow behavior of the coupled system, given the required amount of heat output and thermal characteristics of the soil. Using the theoretical model, a parameter study with respect to tube diameter was conducted to investigate trends applicable to design optimization. The results show that a major part of the pressure drop is caused by gravitation, whereas friction only needs to be considered for small diameter tubes.

**Key Words:** *ground source, heat pump, carbon dioxide, thermosyphon, soil heat exchanger*

## 1 INTRODUCTION

Heat pumps for heating purposes are gaining world wide importance due to an increase in energy efficiency compared to conventional heating methods and the additional possibility of providing cooling during the summer. Air-source heat pumps are the most common heat pumps in the USA due to their ease of installation. However, air-source heat pumps are not the most energy efficient heat pump systems in most cases. Air-source heat pumps achieve seasonal performance factors (SPFs) of approximately 2.5, while ground-coupled heat pumps achieve SPFs of up to 4 or more depending on climate conditions. Due to the increase in SPF, the sale of ground-coupled heat pumps is increasing rapidly, especially in Europe.

Ground-coupled heat pumps use heat-exchangers that are located in the soil to provide a heat source for the heat pump system evaporator. The ground acts as a large thermal reservoir, which remains at a constant temperature throughout the whole year for a depth of 10 m and lower (*Michael Rohm 1999*). Up to now, most ground-source heat pump systems use a brine solution in a secondary fluid loop to extract the heat from the soil. Some systems use horizontally installed fluid loops that are located between 1 and 2 meters below the ground surface. These systems are in the upper layer of the ground and the soil temperature changes during the seasons. Other systems use vertical boreholes in the ground, which can be up to 250 m in depth. Vertical systems require less space and benefit from the constant soil temperature, but they have the disadvantage of a higher power consumption of the brine-pump to overcome the gravitational pressure drop, which increases the electrical energy consumption of the heat pump by up to 15%. Thus, a new concept was introduced several years ago in which a closed CO<sub>2</sub> thermosyphon is used to extract heat from the soil (*Halozan and Rieberer 2002 and 2003*). The system is self-circulating, which eliminates the need for a brine pump and therefore, increases the heat pump efficiency. The thermosyphon is closed and contains only CO<sub>2</sub> (without any oil) which is environmental friendly, non-

toxic and non-flammable unlike most other refrigerants. This means, that there is no risk for any pollution of the soil in case of leakage from the system.

One disadvantage of the CO<sub>2</sub> thermosyphon system is that it cannot be used for cooling during the summertime. The thermosyphon only works in one direction and therefore, cannot be used as a heat sink for a heat pump.

The schematic of a ground-source heat pump system using a CO<sub>2</sub> thermosyphon is shown in Fig. 1. The system is similar to a common single-stage cycle, except that the evaporator is specially designed to extract heat from the thermosyphon condensing section. Figure 2 shows the working principle of the thermosyphon, which can be divided into three sections. The uppermost part is the condenser, which is cooled down by the evaporator of the heat pump. As the temperature in that region decreases, the CO<sub>2</sub> in the system condenses and starts to form a liquid film on the wall, which is drawn downward by gravity. Gas streaming upward in the thermosyphon replaces the condensed vapor. The falling liquid film on the wall is heated up by the soil, which normally has, in an undisturbed area, temperatures around 10°C. This temperature decreases due to heat extraction over time. The film starts to evaporate until it reaches the bottom of the pipe or dry-out occurs. The produced vapor rises to the condensing section on the upper part of the thermosyphon where it is condensed again (see Fig. 2).

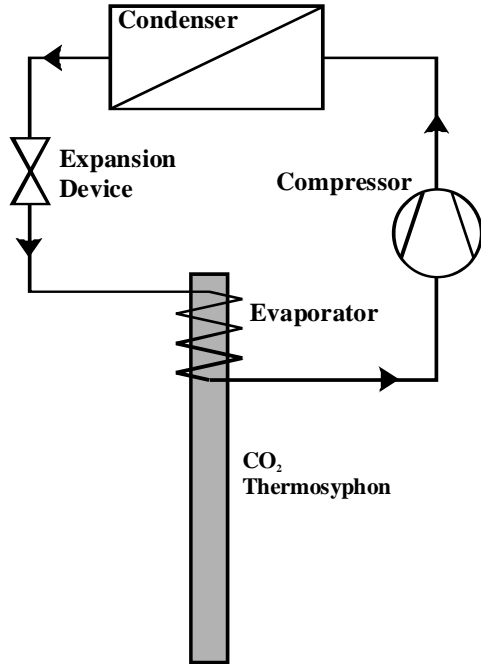


Fig. 1. Schematic of a heat pump with a thermosyphon as heat source

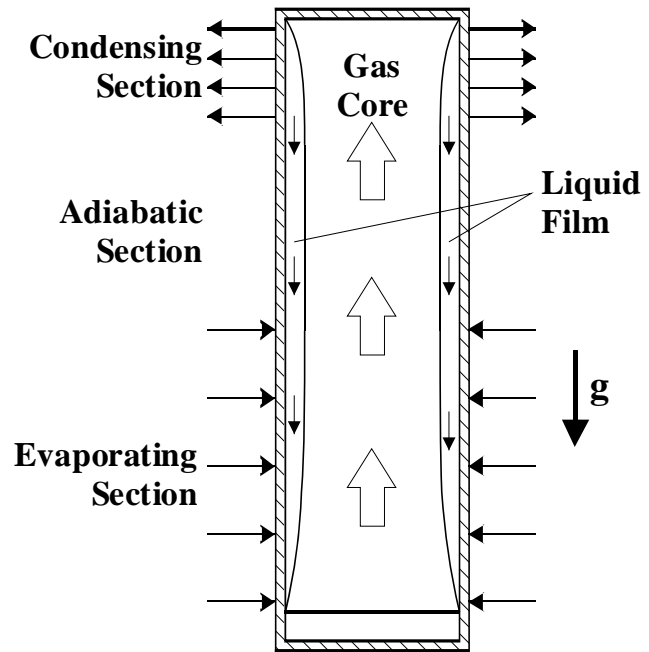


Fig. 2. Principle of the thermosyphon

## 2 PROBLEM DEFINITION

In order to design a thermosyphon for a ground source heat pump application, the attributes of the system such as tube length, diameter, temperature distribution, and pressure drop need to be investigated. The closed thermosyphon consists of three distinct sections: a condensing section at the top, an adiabatic section in the middle and an evaporation section at the bottom. The scope of the numerical model described in this paper was to model the two-phase counter-current annular flow behavior of the coupled system given the required amount of heat output and thermal characteristics of the soil. Once the model was validated, a parameter study was conducted with respect to tube diameter to investigate trends applicable to design optimization.

Several assumptions were made in order to simplify the model without compromising the results. Steady-state operation of the thermosyphon was assumed, in which the mass flow rate of vapor flowing upwards is equal to the mass flow rate of liquid flowing downwards at any cross-section. Also, the thermodynamic equilibrium quality over the cross section of the tube was assumed to be always 0.5 due to steady state operation. Liquid droplet entrainment in the vapor core and wavy liquid-vapor interface were neglected. Finally, different boundary conditions were used for the condensing and evaporating sections in order to secure the stability of the assumptions.

### 3 NUMERICAL MODEL

In order to get a solvable numerical model for the annular flow regime, some simplifications had to be made which will be explained in this paragraph. Afterwards, a code was written using the EES (Engineering Equation Solver) program to solve the numerical problem. The annular flow was modeled separately for the gas core and the liquid film. As a boundary condition for the single-phase vapor core model, the relative velocity of the vapor-liquid surface is calculated as a difference between the velocity of the upward flowing vapor and the velocity of the downward flowing liquid film. With this expression, the interfacial shear stress and pressure gradient can be calculated.

A control volume over the vapor core with radius  $R - \delta$  was used to derive Equations 1 through 3 (refer to Figure 4). The pressure gradient was determined from the conservation of momentum equation for the vapor core. In addition, in order to determine the thermodynamic properties of the  $\text{CO}_2$ , it was assumed that the vapor temperature is at  $T_{\text{sat}}$ .

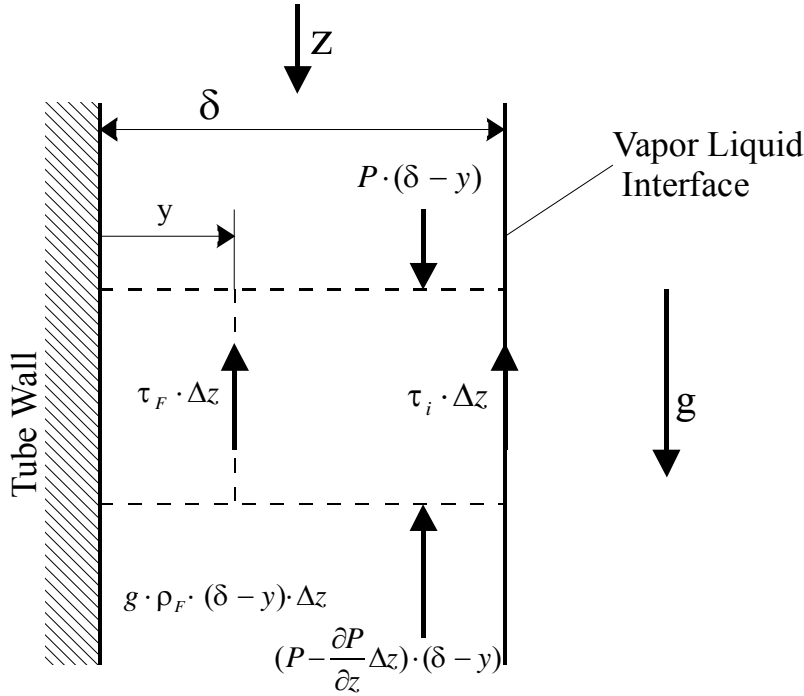
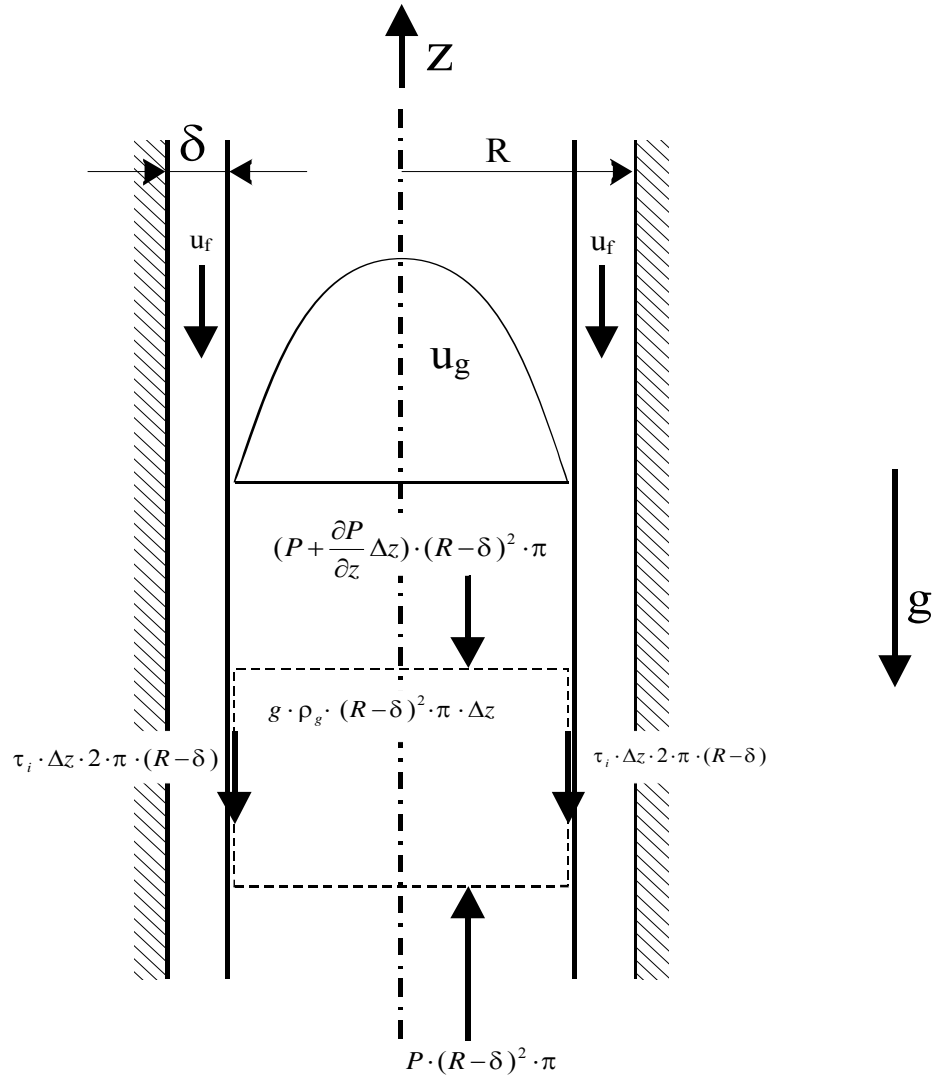


Figure 3. Control volume of the liquid film



**Figure 4. Control volume of the vapor core**

$$\tau_i = \frac{\rho_g (u_g - u_f)^2 c}{2Re^n} \quad (1)$$

Laminar:  $Re < 2300$ ,  $c = 16$ ,  $n = 1$

Transition:  $2300 < Re < 2 \times 10^4$ ,  $c = 0.079$ ,  $n = 0.25$

Turbulent:  $Re > 2 \times 10^4$ ,  $c = 0.046$ ,  $n = 0.2$

$$Re = \frac{2G_g (R - \delta)}{\mu_g} \quad (2)$$

$$-\left(\frac{\partial P}{\partial z}\right) = \left(\frac{4\tau_i}{R - \delta}\right) + \rho_g g \quad (3)$$

To model the liquid film, the effect of the curvature of the wall was neglected since  $R \gg \delta$ . Therefore, the model reduced to a two-dimensional flow over a vertical plate. The model used is similar to the Nusselt solution for laminar condensation on a vertical plate, except it accounts for turbulent effects and interfacial shear stress. Equations 4 and 5 for the film shear stress and velocity, respectively, resulted from a control volume of the liquid film (refer to Figure 3). The (Mudawar and El-Masri 1985) free-falling film turbulence model was implemented for the eddy momentum diffusivity parameter.

$$\tau_f = \mu_f \left( 1 + \frac{\varepsilon_{m,f}}{\nu_f} \right) \frac{du_f}{dy} \quad (4)$$

$$u_f = \int_0^y \left\{ \frac{\left[ -\left( \frac{\partial P}{\partial z} \right) + \rho_f g \right] (\delta - y) - \tau_i}{\mu_f \left( 1 + \frac{\varepsilon_{m,f}}{\nu_f} \right)} \right\} dy \quad (5)$$

Equations 6 and 7 express the mass flow rate per unit width and total mass flow rate of the liquid film, respectively. The heat transfer coefficient is determined using Equations 8 and 9. The turbulent Prandtl number was for simplicity assumed to be a value of 1 as investigated by (Kays and Crawford 1993). The film thickness  $\delta$  was determined from an energy balance analysis.

$$\Gamma_f = \rho_f \int_0^\delta u_f dy \quad (6)$$

$$W_f = 2\pi \left( R - \frac{\delta}{2} \right) \Gamma_f \quad (7)$$

$$h_f = \left\{ \frac{1}{k_f} \int_0^\delta \frac{1}{\left( 1 + \frac{Pr_f \varepsilon_{m,f}}{Pr_{T,f} \nu_f} \right)} dy \right\}^{-1} \quad (8)$$

$$Pr_f = \frac{\nu_f}{\alpha_f}, \quad \alpha_f = \frac{k_f}{\rho_f c_{p,f}} \quad (9)$$

The starting point of the numerical model is at the beginning of the evaporating section. The mass flow rate can be calculated from Equation 10 based on the total heat-flux, which was set to 5 kW in this particular case. The mass flow rate per unit width can then be calculated from Equation 7. In order to calculate the thermodynamic properties of CO<sub>2</sub> at the starting point, the saturation pressure was calculated neglecting the thermal resistance of the liquid film, which is unknown at the starting point, but much less than the thermal resistance of the steel tube and soil. The last input parameter that needs to be determined is liquid film thickness,  $\delta$ , which was solved in an iterative way based on the known flow rate at the exit of the adiabatic section given a fixed error tolerance.

$$W_{f, \text{adiabatic}} = \frac{\dot{Q}_C}{h_{fg} + c_{p,f} (T_w - T_s)} \cong \frac{\dot{Q}_C}{h_{fg}}, \quad h_{fg} \gg c_{p,f} (T_w - T_s) \quad (10)$$

Once the input parameters of the evaporating section are known, the numerical analysis can be carried out stepwise over the whole evaporating section until dryout occurs, i.e., when  $W_f = 0$ . The same process was conducted for the adiabatic and condensing sections based on the given lengths presented in the results section with corresponding changes to the boundary conditions, such as heat flux and tube diameter.

As previously mentioned, two cases were considered for the thermosyphon model corresponding to different boundary conditions. One case considered a constant heat flux in both the condensing and evaporating sections, while the other one used soil temperature data published by (*Michael Rohm 1999*). The soil temperature values per soil depth were decreased by  $5^{\circ}\text{C}$  to account for temperature loss due to heat extraction and then used for the calculation of the evaporating section. The heat flux values could then be determined from the heat transfer coefficient along with the temperature profile across the thermosyphon at each  $\Delta z$ .

The same process mentioned above was used for the adiabatic section except the heat flux was set to zero. Since no condensation or evaporation occurs, the mass flow rate is constant in the adiabatic section. However, the liquid film thickness slightly changes due to property variations caused by pressure drop.

Once the numerical model was constructed, a convergence study with respect to the liquid film thickness was conducted to determine the necessary number of iterations steps to achieve an accurate solution. To confirm the validity of the liquid film thickness results obtained from the model a comparison to the Nusselt laminar film condensation model was conducted. The numerical solution showed about twice the film thickness of the laminar model. This can be justified because the laminar model neglects the effect of turbulence resulting in higher liquid speeds as compared to the numerical model. Another confirmation of the numerical prediction was achieved by comparing the soil temperature results from the constant heat flux case to the soil temperature data presented by (*Michael Rohm 1999*) which showed good agreement.

## 4 RESULTS

The results presented here use a constant heat flux as the boundary condition in the condensing section and the soil temperature model for the evaporating section. These assumptions work well although there are some limitations, especially in the evaporating section as the soil model does not account for temperature changes due to the heat extraction over an extended period of time. The following results were calculated for a tube diameter of 200 mm in the condensing section which has a length of 2m. The diameter of the adiabatic and evaporating section was varied in 4 steps from 12 mm to 60 mm.

Figure 5 presents the saturation temperature as a function of the tube depth. As can be seen from Figure 5, the saturation temperature is the highest for the largest diameter. This can be explained through the higher heat transfer area for a large diameter tube, which leads to a better coupling to the soil temperature which increases from  $6^{\circ}\text{C}$  in 10 m depth to  $9^{\circ}\text{C}$  in 100 m depth as explained earlier. The increase of the saturation temperature towards larger depths is caused by the pressure drop of the up-streaming vapor core, as shown in Figure 6, which presents the pressure drop as a function of the tube depth. In addition, it can be seen throughout Figures 5 through 9 that the tube with the smallest diameter needs the largest depth, whereas in larger diameter tubes onset of dryout occurs in shorter depths.

It can also be seen from Figure 6 that the pressure drop in the tube with the smallest diameter is the largest. The pressure drop of the vapor core consists of two parts. One is the gravitational pressure drop which is almost constant at around 1 kPa/m and changes due to the variation in material properties according to the  $\text{CO}_2$  temperature. The second part of the pressure drop is caused by friction and depends greatly on the tube diameter. An inner diameter of 12 mm for the evaporating and adiabatic sections is actually the lower limit for a functioning thermosyphon. When the diameter is further reduced, flow reversal occurs and the system does not function any longer as intended. The frictional pressure loss is the largest for the adiabatic section where the mass-flow-rate and liquid film thickness are the highest. As mentioned before, the diameter of the condensing section is much larger than the rest of the thermosyphon because the heat-flux per unit length is much higher in

the condensing section. In a real system the condenser (sometimes called header) might have a different shape with an increased effective area which is not implemented in this simulation. An additional detail about the gravitational pressure drop per unit length is that the gravitational pressure drop increases as the tube diameter increases. This is caused by the higher temperature and pressure of the CO<sub>2</sub> at larger tube diameters, which leads to a higher density.

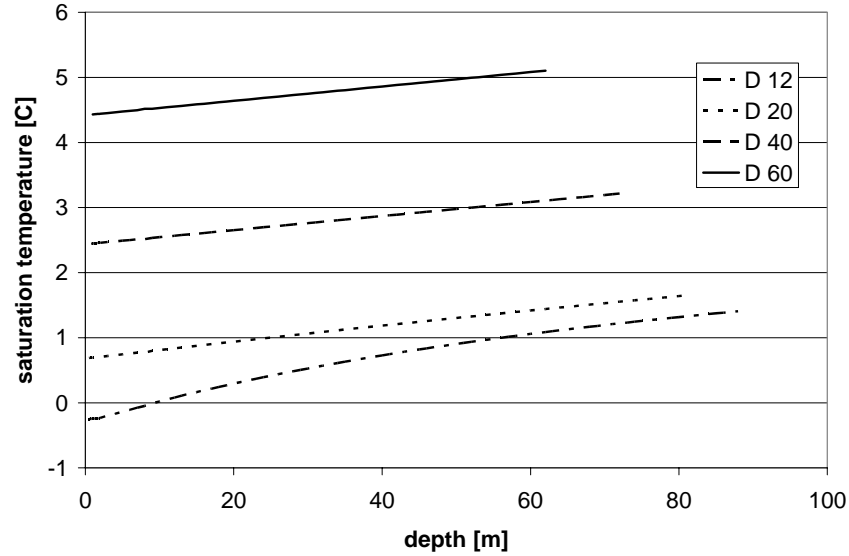


Fig. 4. Saturation temperature of CO<sub>2</sub>

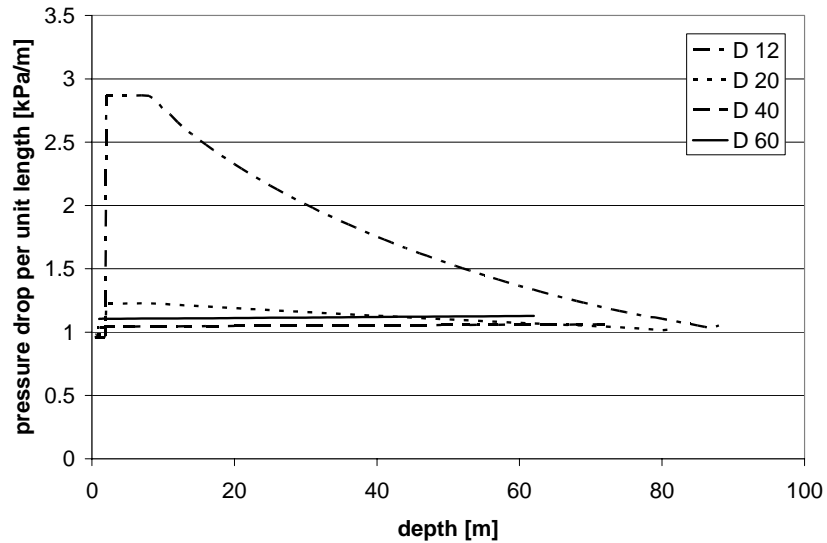
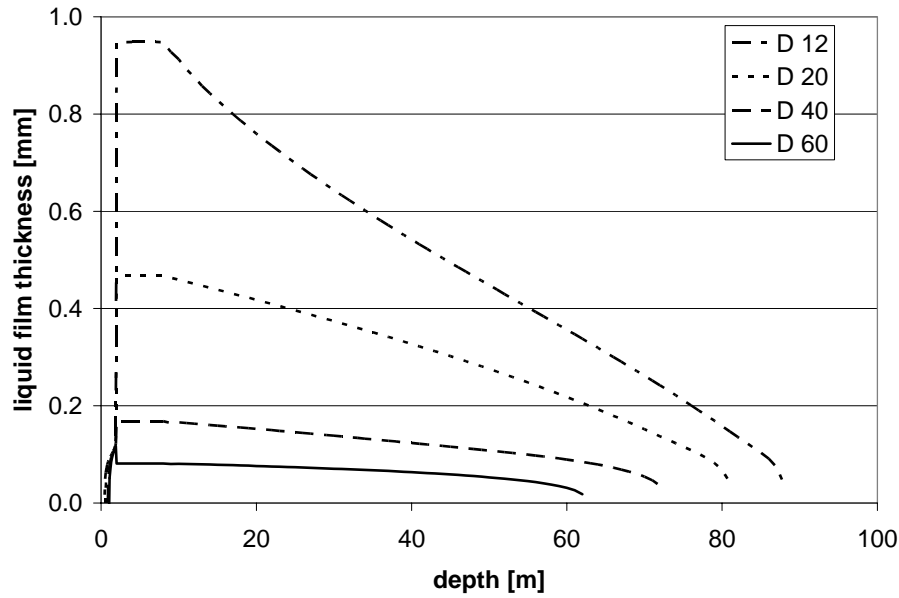


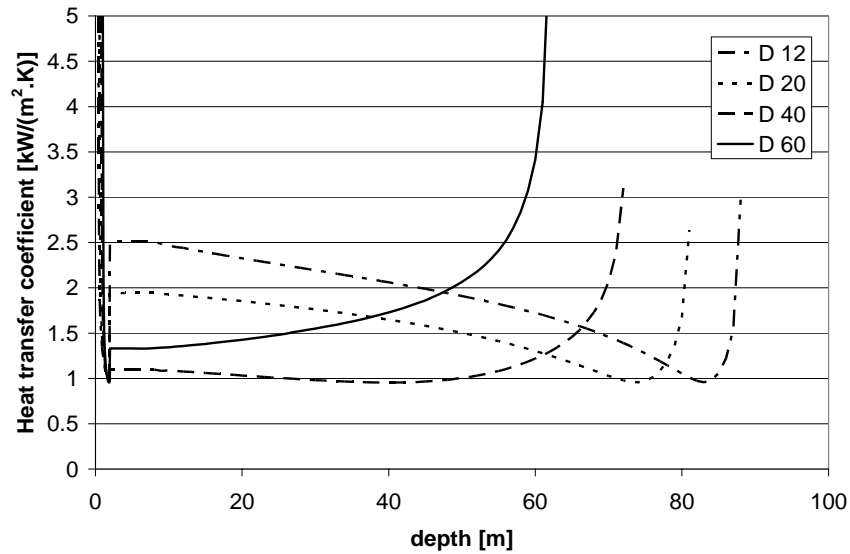
Fig. 6. Pressure drop along the tube

Figure 7 shows the thickness of the falling liquid film as a function of tube depth. The film thickness increases with a decrease in tube diameters. Especially for the smallest diameter tube, the increase in film thickness is significant as the effect of the greater shear stress at the liquid-vapor interface leads to low liquid flow velocities. In addition, the film thickness decreases with the tube depth as more and more of the CO<sub>2</sub> evaporates. At a certain depth the liquid film thickness approaches zero and dryout occurs. This depth is 65 m for the tube with an inner diameter of 60 mm and 90 m for the tube with an inner diameter of 12 mm.

It can be seen from Figure 8 that the convective heat transfer coefficient of the liquid film increases with decreasing film thickness. Contrary to this effect is the fact that a thinner liquid film has a lower flow velocity which increases the thermal resistance of the liquid film.



**Figure 7: Thickness of the free falling liquid film**



**Fig. 8. Heat transfer coefficient of the liquid film**

Figure 9 shows the average speed of the liquid film and the vapor core. Due to the small mass flow rate of the refrigerant the speed is relatively low given the small diameter of the thermosyphon. The vapor speed is positive as it flows in the upward direction and the liquid speed is negative as it is pulled downward by gravity. The speed reaches a maximum for both phases in the adiabatic section where the refrigerant mass flow rate is the highest. This is due to the fact that immediately after the adiabatic section the refrigerant starts to evaporate and the refrigerant flow rate decreases. In the condensing section the flow rate reduces corresponding to the condensed vapor. The average speed of the vapor decreases almost linearly due to the almost constant wall heat flux. The large step in speed after the condensing section is caused by the increase of the tube diameter to 200 mm. The velocity of the vapor core is the largest for the smallest diameter tube, as expected. The liquid film velocity follows the same trend with one exception: For the tube with 12 mm diameter, the liquid speed is



smaller at the beginning of the evaporating section, which is due to the higher shear stress on the vapor-liquid interface. This shear stress slows the liquid film down and increases the thickness of the liquid film.

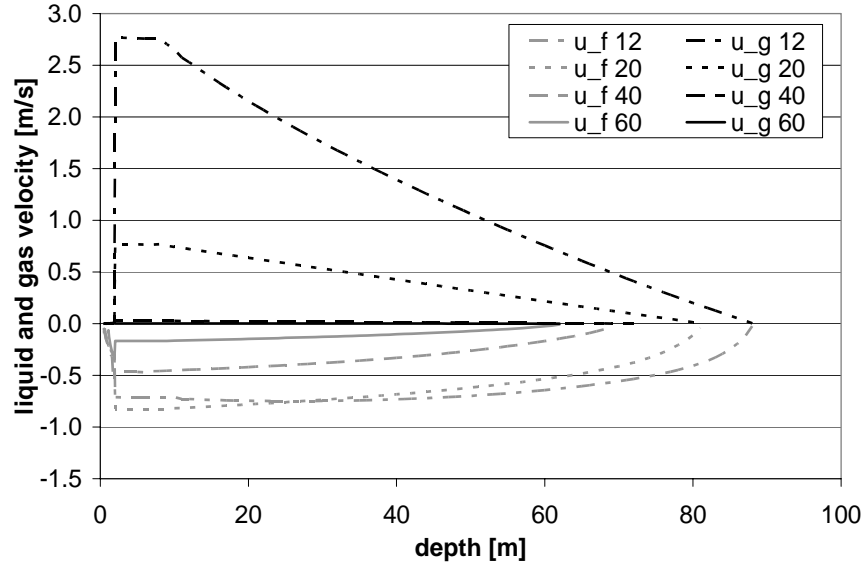


**Figure 9: Velocity of the free falling liquid film and the up-streaming gas core**

Figure 10 presents the local velocity of the falling liquid film for the tube with 20 mm inner diameter at the end of the adiabatic section versus the ratio of the wall distance over the liquid film thickness. This location was chosen since the mass-flow-rate is highest at this point and therefore, the film thickness is at its maximum. As can be seen from this figure, the velocity of the liquid at the wall is 0 and has a high gradient near the wall. In the middle of the film the profile is almost flat due to the occurrence of turbulent flow. The gradient at the vapor-liquid interface shows the effects of the shear stress between the vapor and the liquid. This effect increases for smaller tube diameters and can lead to flow reversal.

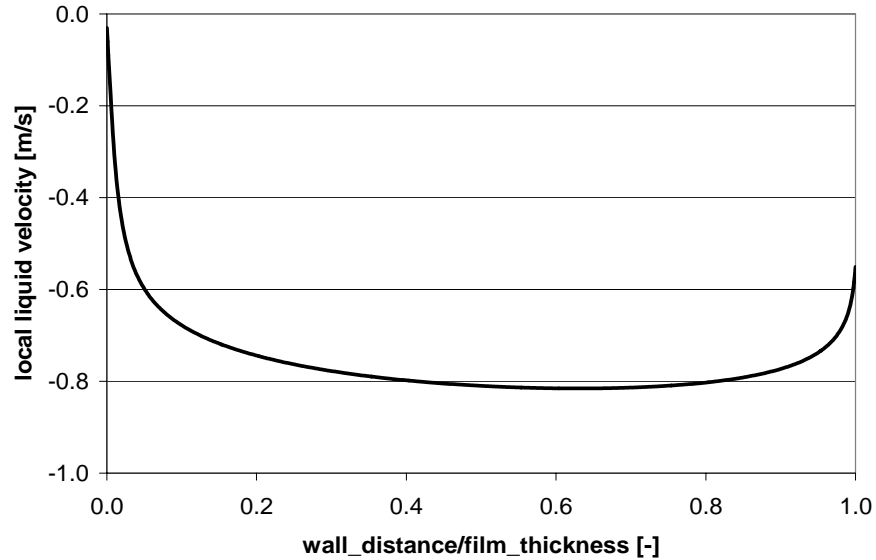


**Figure 10: Local velocity of the falling liquid film**

## 5 CONCLUSIONS

CO<sub>2</sub> thermosyphons for ground-source heat pump applications are a promising option as the soil heat-exchanger. Unlike common brine systems, a pump to circulate the secondary fluid is not required. In

addition, the temperature difference between the soil and the evaporator of the heat pump can be reduced which leads to higher performance. The CO<sub>2</sub> thermosyphon system also solves environmental problems of other soil heat exchangers with respect to pollution of the soil and groundwater in case of leakage since CO<sub>2</sub> is a natural gas. A numerical model has been developed and is presented here, which predicts several parameters of the CO<sub>2</sub> thermosyphon in the condensing, adiabatic and evaporating section. The model can be used to design a CO<sub>2</sub> thermosyphon, such as diameter and length, for given operating conditions, such as soil temperature and heat load. By incorporating a slight enhancement in the model, it can also be used to predict the required refrigerant charge in the thermosyphon.

A major problem encountered while conducting this project was the lack of literature for this particular application. No experimental data was available to validate the numerical model for a CO<sub>2</sub> thermosyphon. However, a comparison of the model prediction to experimental results of a vertical brine heat-exchangers showed reasonable agreement. A second validation was made by comparing the model predictions with results obtained by using the Nusselt model to calculate the film thickness. This comparison also showed reasonable agreement. One of the main results obtained from the numerical model was that the liquid film is very thin, i.e., the maximum film thickness is approximately 1 mm. This can be explained by the fact that the viscosity of CO<sub>2</sub> is approximately 10 times smaller than that of water, which leads to a higher gradient in the liquid film velocity and therefore, to a thinner liquid film.

One of the main observations of the numerical model predictions was that the gravitational pressure drop has a far greater effect on the pressure profile along the tube than the frictional pressure drop, except for the smallest diameter tube. This is due to the low flow velocities. In addition, no significant difference could be found between the boundary conditions of constant heat-flux and given soil temperatures along the tube. Another interesting result is that tubes with smaller diameters can be used for the adiabatic and evaporating sections, which account for the majority of the thermosyphon length. The diameters for brine systems with comparable heat output would be significantly larger. In addition to using smaller diameter tubes, the temperature difference between the soil and heat pump evaporator is smaller for a CO<sub>2</sub> thermosyphon compared to a brine system, which leads to a higher heat pump evaporating temperature. This increase in temperature produces a higher efficiency of the overall system.

The model could be improved by using a more accurate treatment of the tube and soil interface as it pertains to thermal resistance. One option would be to use a thermal storage model for the surrounding soil. However, this might be difficult to incorporate due to the variety of soil characteristics corresponding to different site locations. In addition to different load conditions of the soil, there are other parameters, such as different rock materials, aquifers, etc., which can only be identified by conducting measurements at the specific location. Future work should focus on the design of the condensing section (header) and a transient model for the startup of the closed CO<sub>2</sub> thermosyphon.

## 6 NOMENCLATURE

Symbol		Subscripts	
$\Delta$	Condensation film thickness	f	Fluid
$\varepsilon_m$	Eddy momentum diffusivity	g	Gas
$\Gamma$	Mass flow rate per unit width	i	Interfacial
M	Absolute viscosity	s	Soil
P	Density	t	Turbulent
T	Shear stress	w	Wall
N	Kinematic viscosity		
G	Gravitational constant		
H	Thermal convection coefficient		
G	Mass velocity		
P	Pressure		
Q	Heat flux		
R	Inner radius of the thermosyphon		

U	Velocity
W	Mass flow rate
Z	Depth below the surface of the soil

## 7 REFERENCES

El-Masri M. A., Mudawar I. A., Momentum and Heat Transfer Across Freely-Falling Turbulent Liquid Films, *International Journal of Multiphase Flow* 12 (1985) 771-790.

Halozan Hermann, Rieberer Rene, Bangheri Andreas, Direct-Expansion Ground-Coupled Heat Pumps, 21st International Congress of Refrigeration, Washington (2003).

Hepbasli Arif, Akdemir Ozay, Hanicioglu Ebru, Experimental Study of a Closed Loop Vertical Ground Source Heat Pump System, *Energy Conversion and Management* 44 (2003) 527-548.

Hepbasli Arif, Performance Evaluation of a Vertical Ground-Source Heat Pump System in Izmir, Turkey, *International Journal of Energy Research*, 26 (2002) 1121-1139.

Kays W.M., M.E. Crawford, *Convective Heat and Mass Transfer*, McGraw-Hill Inc., 3rd Edition, (1993).

Reed J. G., Tien C. L., Modeling of the Two-Phase Closed Thermosyphon, *Transactions of the ASME Journal of Heat Transfer* 109, 3 (1987) 722-730.

Rieberer Rene, Mittermeyer Karl, Halozan Hermann, CO<sub>2</sub> Heat Pipe for Heat Pumps, *Proceeding of the 5<sup>th</sup> IIR-Gustav Lorentzen Conference on Natural Working Fluids*, China, 2002, p200-207.

Rohm Michael, *Das System Erdwaerme-Waermepumpe-Heizkreislauf – eine interdisziplinaere Aufgabe*, ECOS – Umwelttechnische und Wissenschaftliche Publikationen, (1999)